Journal of Molecular Structure 1024 (2012) 1–12

Contents lists available at SciVerse ScienceDirect

Journal of Molecular Structure

journal homepage: www.elsevier.com/locate/molstruc

The spectroscopic (FTIR, FT-Raman, UV and NMR), first-order hyperpolarizability and HOMO–LUMO analysis of 4-amino-5-chloro-2-methoxy-benzoic acid

A. Poiyamozhi [a], N. Sundaraganesan [b,*], M. Karabacak [c], O. Tanrıverdi [c], M. Kurt [d]

[a] Department of Physics, Government Arts College, Dharmapuri 636 705, India
[b] Department of Physics (Engg.), Annamalai University, Annamalai Nagar 608 002, Chidambaram, Tamil Nadu, India
[c] Department of Physics, AfyonKocatepe University, 03040 Afyonkarahisar, Turkey
[d] Department of Physics, Ahi Evran University, 40100 Kırsehir, Turkey

HIGHLIGHTS

- The FTIR and FT-Raman spectra of 4A5Cl2MBA were recorded.
- The vibrational frequencies were calculated for monomer and dimer by DFT method.
- NMR and UV–Vis spectra were also recorded and compared with calculated ones.

ARTICLE INFO

Article history:
Received 31 January 2012
Received in revised form 2 May 2012
Accepted 3 May 2012
Available online 12 May 2012

Keywords:
TD-DFT
Vibrational spectra
PES scan analysis
First order hyperpolarizability
NMR
4-Amino-5-chloro-2-methoxybenzoic acid

ABSTRACT

The solid phase FTIR and FT–Raman spectra of 4-amino-5-chloro-2-methoxybenzoic acid (4A5Cl2MBA) have been recorded in the regions 400–4000 and 50–4000 cm^{-1}, respectively. The spectra have been interpreted in terms of fundamentals modes, combination and overtone bands. The structure of the molecule has been optimized and the structural characteristics have been determined by density functional theory (B3LYP) method with 6-311++G(d,p) as basis set. The vibrational frequencies were calculated for most stable conformer and were compared with the experimental frequencies, which yield good agreement between observed and calculated frequencies. The infrared and Raman spectra have also been predicted from the calculated intensities. ^{1}H and ^{13}C NMR spectra were recorded and ^{1}H and ^{13}C nuclear magnetic resonance chemical shifts of the molecule were calculated using the gauge independent atomic orbital (GIAO) method. UV–Visible spectrum of the compound was recorded in the region 200–400 nm and the electronic properties HOMO and LUMO energies were measured by time-dependent TD-DFT approach. Nonlinear optical and thermodynamic properties were interpreted. All the calculated results were compared with the available experimental data of the title molecule.

1. Introduction

Derivatives of benzoic acid have been the subject of investigation for many reasons. Derivatives of benzoic acid are essential components of the vitamin B-complex. Benzoic acid occurs widely in plants and animals tissues along with vitamin B-complex and is used in miticides, contrast media in urology, cholocystographic examinations and in the manufacture of pharmaceuticals. Methoxybenzoic acids (anisic acids) are naturally occurring compounds and their biological activity is widely described. They are known to be important inhibitors in the growth of bacteria [1] and they influence the catalytic activity of many enzymes [2]. The amino benzoic acids belong to aromatic amino acids, which are biologically active substances [3]. 4-aminobenzoic acid is a non-protein amino acid that is widely distributed in nature. Most often it is used in sunscreen preparations, since it can help to protect the skin against ultra-violet radiation.

In the previous work, molecular structure and charge density analysis of p-methoxybenzoic acid have been made by Fausto et al. [4]. Experimental and theoretical IR, Raman, NMR spectra of 2-, 3- and 4-aminobenzoic acids have been investigated by Samsonowicz et al. [5]. Sundaraganesan et al. [6,7] studied the vibrational spectra and assignments of 5-amino-2-chlorobenzoic acid and p-chlorobenzoic acid by HF and DFT methods. Molecular structure, vibrational assignments and proton NMR analysis of o-, m- and p-methoxybenzoic acids have been carried out by

* Corresponding author. Tel.: +91 9442068405.
E-mail address: sundaraganesan_n2003@yahoo.co.in (N. Sundaraganesan).

0022-2860/$ - see front matter © 2012 Elsevier B.V. All rights reserved.
http://dx.doi.org/10.1016/j.molstruc.2012.05.008

Kalinowska et al. [8]. To the best of our knowledge, neither the experimental nor theoretical studies of the title compound of 4-amino-5-chloro-2-methoxybenzoic acid have been available until now.

In this paper, we reported the experimental and theoretical studies on 4-amino-5-chloro-2-methoxybenzoic acid. The interaction energies, NMR spectral analysis, molecular electrostatic potential, thermodynamic and nonlinear optical properties of the title compound were investigated at the B3LYP/6-311++G(d,p) level.

2. Spectral measurements

The 4-amino-5-chloro-2-methoxybenzoic acid sample was purchased from Sigma–Aldrich Chemical Company with a stated purity 97% and it was used as such without further purification. The sample was prepared using a KBr disk technique because of solid state. The FTIR spectrum of molecule recorded in the region 400–4000 cm^{-1} on a Perkin Elmer FTIR spectrometer calibrated using polystyrene bands. FT-Raman spectrum of the sample recorded using 1064 nm line of Nd:YAG laser as excitation wave length in the region 50–4000 cm^{-1} on a Bruker RFS 100/S FT-Raman spectrometer. The detector is a liquid nitrogen cooled Ge detector. Five hundred scans were accumulated at 4 cm^{-1} resolution using a laser power of 100 mW.

The ultraviolet absorption spectra of 4-amino-5-chloro-2-methoxybenzoic acid dissolved in ethanol and DMSO were examined in the range 200–400 nm using Shimadzu UV-1800 PC, UV–Vis recording Spectrometer. Data were analyzed by UV PC personal spectroscopy software, version 3.91.

NMR experiments were performed in Bruker DPX 600 MHz at 300 K. The compound was dissolved in DMSO. Chemical shifts were reported in ppm relative to tetramethylsilane (TMS) for ^{1}H, ^{13}C NMR and DEPT 135 spectra. ^{1}H and ^{13}C NMR spectra were obtained at a base frequency of 600 MHz and 150 MHz, respectively.

3. Computational details

The molecular geometry is directly taken from the X-ray diffraction experimental result without any constraints. The DFT calculations were performed using the Gaussian 03 program package [9]. The calculations employed the B3LYP exchange–correlation functional, which combines the hybrid functional of Becke [10,11] with the gradient–correlation functional of Lee et al. [12] and the split-valence polarized 6-311++G(d,p) basis set [13]. The harmonic vibrational frequencies were calculated at the same level of theory for the optimized structures. Vibrational band assignments were made using the Gauss-View molecular visualization program [14]. Additionally, the calculated vibrational frequencies were clarified by means of the total energy distribution (TED) analysis and assignments of all the fundamental vibrational modes by using VEDA 4 program [15]. After optimization, ^{1}H and ^{13}C NMR chemical shifts were calculated using the GIAO method [16] in DMSO. UV–Vis spectra, electronic transitions, vertical excitation energies, absorbance and oscillator strengths were computed with the time-dependent DFT method. The electronic properties such as HOMO and LUMO energies were determined by TD-DFT approach. To investigate the reactive sites of the title compound the MEP were evaluated using the B3LYP/6-311++G(d,p) method.

4. Prediction of Raman intensities

The Raman activities (S_{Ra}) calculated with Gaussian 03 program [9] converted to relative Raman intensities (I_{Ra}) using the following relationship derived from the intensity theory of Raman scattering [17,18],

$$I_i = \frac{f(v_0 - v_i)^4 S_i}{v_i[1 - \exp(-hcv_i/kT)]}$$

where v_0 is the laser exciting wavenumber in cm^{-1} (in this work, we have used the excitation wavenumber $v_0 = 9398.5\ cm^{-1}$, which corresponds to the wavelength of 1064 nm of a Nd:YAG laser), v_i the vibrational wavenumber of the ith normal mode (cm^{-1}), while S_i is the Raman scattering activity of the normal mode v_i. f (is a constant equal to 10^{-12}) is a suitably chosen common normalization factor for all peak intensities. h, k, c and T are Planck and Boltzmann constants, speed of light and temperature in Kelvin, respectively.

5. Results and discussion

5.1. Potential energy surface scan analysis

On the basis of the definition of the standard conformer, theoretically, 4A5Cl2MBA has four different possible conformers; the structures of all the conformers are shown in Fig. 1. The relative energies of the conformers calculated by B3LYP/6-311++G(d,p) method are collected in Table 1. Possible conformers of 4A5Cl2MBA depend on the rotation of C1—C18 bond, linked to carboxyl group and benzene ring. This bond is responsible for the flexibility and conformational stability of 4A5Cl2MBA. Thus, O19—C18—C1—C6 dihedral angle is a coordinate related to conformational flexibility. The potential energy surface (PES) of the dihedral angle O19—C18—C1—C6, calculated at the B3LYP level of theory, is displayed in Fig. 2. The internal rotational profile of C1—C18 bond was obtained at B3LYP level of theory by allowing the torsional coordinate to vary in steps of 10° from 0° to 360°. This rotation bond yielded the energetically two local minima at 0° and 360°, with $E = -1050.501302$ Hartree for conformer 1 (Fig. 2-C1). For the O19—C18—C1—C6 rotation, the maximum energy (-1050.485157 Hartree) was obtained at 180° (C4) in the potential energy curve. The conformation C2 and C3 corresponds to the dihedral angle of 135° and 90° respectively. It is evident that conformer 1 is the most stable form. The less stable form is conformer 4

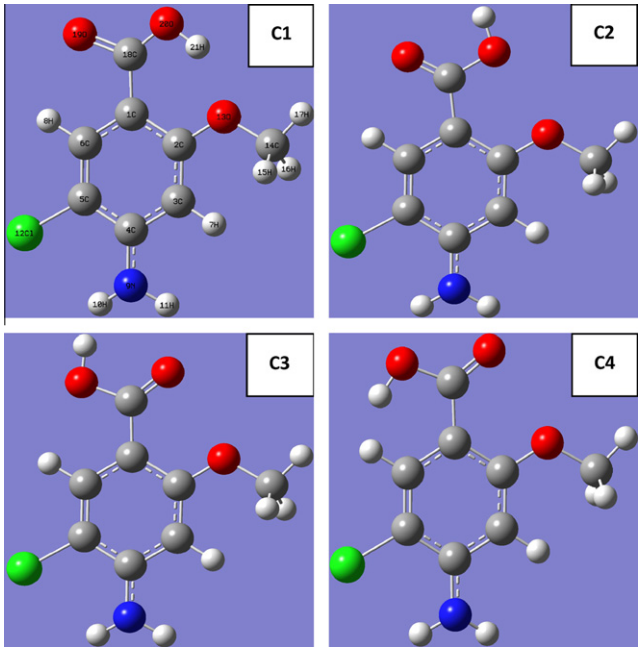

Fig. 1. Theoretical optimized possible geometric structure with atoms numbering of 4A5Cl2MBA.

Table 1
Calculated energies and energy difference for four conformers of 4A5Cl2MBA by DFT method.

Conformers	B3LYP6-311++G(d,p)		
	Energy (hartree)	Energy (kcal/mol)	[a]Energy differences (kcal/mol)
C1	−1050.501302	−659199.0215	0.0000
C2	−1050.488781	−659191.1645	7.8570
C3	−1050.487380	−659190.2853	8.7362
C4	−1050.485157	−659188.8904	10.1311

[a] Energies of the other three conformers relative to the most stable C1 conformer.

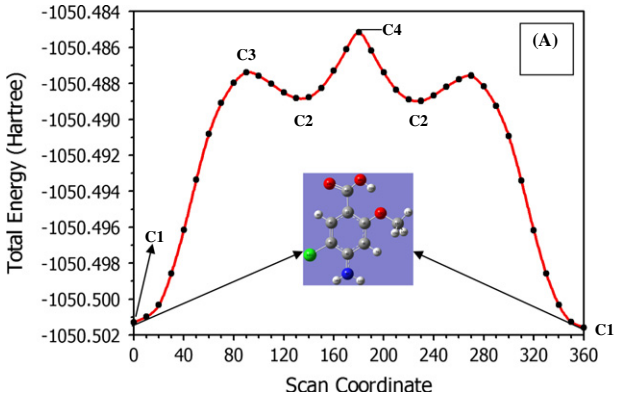

Fig. 2. PES scan for dihedral angle O19—C18—C1—C6 of 4A5Cl2MBA at B3LYP/6-311++G(d,p).

Table 2
The calculated geometric parameters of 4A5Cl2MBA, bond lengths in angstrom (Å) and angles in degrees (°).

Bond lengths	B3LYP	X-ray[a]	Bond angles	B3LYP	X-ray[a]
C(1)—C(2)	1.412	1.386	C(2)—C(1)—C(6)	117.3	118.8
C(1)—C(6)	1.399	1.394	C(2)—C(1)—C(18)	126.5	120.9
C(1)—C(18)	1.502	1.463	C(6)—C(1)—C(18)	116.2	120.3
C(2)—C(3)	1.389	1.384	C(1)—C(2)—C(3)	121.0	121.2
C(2)—O(13)	1.373	1.354	C(1)—C(2)—O(13)	117.0	115.5
C(3)—C(4)	1.406	1.390	C(3)—C(2)—O(13)	122.0	124.5
C(3)—H(7)	1.082	0.979	C(2)—C(3)—C(4)	121.2	121.2
C(4)—C(5)	1.407	1.392	C(2)—C(3)—H(7)	120.6	120.4
C(5)—C6)	1.379	1.370	C(4)—C(3)—H(7)	118.1	119.7
C(6)—H(8)	1.082	0.958	C(3)—C(4)—C(5)	117.5	119.2
O(13)—C(14)	1.428	1.432	C(4)—C(5)—C(6)	121.1	120.2
C(14)—H(15)	1.093	1.004	C(1)—C(6)—C(5)	121.9	120.6
C(14)—H(16)	1.094	1.043	C(1)—C(6)—H(8)	117.6	120.3
C(14)—H(17)	1.088	1.007	C(5)—C(6)—H(8)	120.6	119.1
C(18)—O(19)	1.207	1.254	C(2)—O(13)—C(14)	120.3	118.2
C(18)—C(20)	1.349	1.288	O(13)—C(14)—H(15)	110.9	110.2
O(20)—H(21)	0.973	1.091	O(13)—C(14)—H(16)	110.9	111.5
C(5)—Cl(12)	1.762		O(13)—C(14)—H(17)	105.7	107.2
C(4)—N(9)	1.374		C(1)—C(18)—O(19)	122.0	120.4
			C(1)—C(18)—O(20)	117.8	117.7
			O(19)—C(18)—O(20)	120.2	121.9
			C(18)—O(20)—H(21)	109.8	111.7
			H(15)—C(14)—H(16)	110.2	112.8

[a] Taken from Ref [4].

(Fig. 2-C4) making an angle at 180° with $E = -1050.485157$ Hartree. Therefore, in the present work we have focused on the most stable conformer C1 form of 4A5Cl2MBA molecule to clarify molecular structure and assignments of vibrational spectra.

5.2. Structural analysis

The optimized structural parameters such as bond length and bond angle for the thermodynamically preferred geometry of 4A5Cl2MBA for monomer are determined at B3LYP/6-311++G(d,p) level. The optimized parameters are presented in Table 2 in accordance with the atom numbering scheme of the molecule shown in Fig. 1. The molecules are linked by short intermolecular and asymmetric O—H···O hydrogen bonds of 1.82 Å between oxygen atom and hydrogen atom of hydroxyl group of another molecule to give rise to a dimer. Then, in order to test the effect of intermolecular interactions, the 4A5Cl2MBA dimer formed by O—H···O intermolecular hydrogen bonds is investigated by theoretical methods. The geometry of the molecule under investigation is considered by possessing C_1 point group symmetry. To the best of our knowledge, exact experimental data of the geometrical parameters of 4A5Cl2MBA are not available in the literature. Therefore, our optimized structural parameters are compared with the XRD data of closely related molecule p-methoxybenzoic acid [4]. From the structural data, it is observed that the C1—C2, C3—C4 and C4—C5 bond lengths of ring carbon atoms are larger than that of other ring carbon atoms and also there is a considerable difference between the experimental and theoretical bond lengths. This is due to the substitution of electron donor and electron acceptor groups in the benzene ring and also the presence of intermolecular hydrogen bonding. The calculated bond length of C1—C18 (1.502 Å) is more deviated from the experimental bond length (1.463 Å) due to the presence of intermolecular interaction between carboxyl groups of two different molecules. Because of the electron donating and accepting substituents on the benzene ring, the symmetry of the ring is distorted.

5.3. Vibrational assignments

The vibrational spectrum is mainly determined by the modes of the free molecule observed at higher wavenumbers, together with the lattice (translational and vibrational) modes in the low wavenumber region. In our present study, we have performed a frequency calculation analysis to obtain the spectroscopic signature of 4-amino-5-chloro-2-methoxybenzoic acid. The 4A5 Cl2MBA molecule consists of 21 atoms therefore they have 57 vibrational normal modes. All the frequencies are assigned in terms of fundamental, overtone and combination bands. Assignments have been made on the basis of relative intensities, energies, line shape and total energy distribution (TED). The measured (FTIR and FT-Raman) wavenumbers and assigned wavenumbers of the some selected intense vibrational modes calculated at the B3LYP level using basis set 6-311++G(d,p) along with their TED are given in Table 3. For B3LYP with 6-311++G(d,p) basis set, the wavenumbers in the ranges from 4000 to 1700 cm^{-1} and lower than 1700 cm^{-1} are scaled with 0.958 and 0.983, respectively [19]. The calculated Raman and IR intensities were used to convolute each predicted vibrational mode with a Lorentzian line shape with a full width at half maximum (FWHM = 10 cm^{-1}) to produce simulated spectra. This reveals good correspondence between theory and experiment in main spectral features. The experimental and theoretical FTIR and FT-Raman spectra are shown in Figs. 3 and 4.

Table 3
The observed FT-IR, FT-Raman and calculated wavenumbers (cm^{-1}) using B3LYP/6-311++G(d,p) along with IR and Raman relative intensities, Raman scattering activities, and total energy distribution (TED) of 4A5Cl2MBA.

Mode Nos.	Experimental		B3LYP/6-311++G(d,p)					Assignments based on TED (⩾10%)
	FTIR	FT-Raman	Unscaled	Scaled	[a]I_{IR}	[b]S_{Ra}	[c]I_{Ra}	
1	3459s		3701	3545	40.14	46.49	20.25	υ_{asym} NH_2 (100)
2	3345s	3348w	3641	3488	271.22	24.67	11.35	υ OH (100)
3	3240s	3228w	3589	3438	67.57	207.11	100.01	υ_{sym} NH_2 (100)
4			3211	3076	7.34	58.67	40.09	υ CH (99)
5		3078m	3201	3067	4.37	69.58	47.96	υ CH (99)
6	3019vw	3015w	3146	3014	11.50	106.00	76.86	υ_{asym} CH_3 (100)
7	2947ms	2946w	3092	2962	24.06	51.34	39.13	υ_{asym} CH_3 (100)
8		2839w	3024	2897	43.45	166.86	135.36	υ_{sym} CH_3 (100)
9	1710vs	1705s	1795	1719	423.05	99.78	265.54	υ C═O (88)
10	1639s	1643m	1659	1631	416.46	91.91	269.82	ρ NH_2(65) + υ CC (20)
11	1609s	1612s	1632	1605	78.59	81.47	246.32	υ CC(45) + ρNH_2(32)
12	1593s	1592w	1593	1566	20.61	3.29	10.40	υ CC (69) + βCNH (12)
13	1512w	1513w	1530	1504	47.99	14.78	50.21	υ CC(33) + βCH (31) + υ CN(10)
14		1484w	1504	1478	75.92	3.93	13.77	ρ CH_3(62) + ΓCOCH (17)
15			1493	1468	11.40	12.17	43.13	ρ CH_3(77) + ΓCOCH (23)
16	1460m	1455w	1486	1461	8.74	2.31	8.26	ω CH_3(80)
17	1427w	1427m	1447	1422	208.37	5.49	20.56	υ CC(30) + ωCH_3(10) + βHCO (10)
18	1369s		1405	1381	357.30	4.25	16.73	β OH (80)
19	1334m	1339w	1349	1326	6.58	1.31	5.52	υ CC(82) + βCNH(11)
20		1322w	1328	1305	118.89	34.52	149.31	υ CC (40) + υ CN (26) + β CH(10)
21	1248w	1265vs	1280	1258	74.48	1.18	5.42	β CH (83)
22	1209m	1230m	1230	1209	225.40	5.07	24.82	υ CO (35) + r CH_3(30)
23			1222	1201	160.51	63.58	314.51	υ $C_{18}O_{20}$(30) + υ $C_{18}C$(22) + r CH_3(13)
24	1173w	1173vw	1195	1174	42.07	17.50	89.74	r CH_3(29) + β CCH(27) + υ CO(16) + υ CC(11)
25			1168	1148	0.58	2.38	12.64	t CH_3(86) + Γ COCH (14)
26		1111w	1119	1100	33.62	1.87	10.61	υ C—O (42) + υ CC(14) + β CNH (10)
27			1085	1067	0.31	2.03	12.07	β CNH (62) + υ CC(18)
28	1049s	1048w	1069	1051	10.85	1.02	6.20	υ C_{14}—O(36) + υ CC(15) + β CCC(11) + β CH(11) + υ C—Cl(10)
29	982s	982w	998	981	45.21	8.80	59.30	υ CO(46) + υ CC(13) + υ CN(10)
30	902m	903w	950	934	13.78	0.23	1.67	Γ CH (90)
31	820s	799w	814	800	29.78	0.25	2.26	Γ CH (71) + Γ CCCC (10)
32	771w		794	781	37.26	0.69	6.44	β OCO (18) + υ C18—C(18) + υ C_{18}—O(14)
33		740s	770	757	3.28	0.28	2.73	Γ CCCO(60) + Γ HOCO (25)
34	738w		746	734	2.60	24.04	244.29	υ CC(35) + β CCC(33)
35	689m	668w	691	679	0.50	1.10	12.43	Γ CCCC(33) + Γ HCCC (28) + Γ CCNH (11) + Γ CCNCl (10)
36	666w		664	653	35.97	0.56	6.67	ρ CO_2 (30) + υ C—Cl (18) + β CCO (15) + β CCC(14)
37	650w	641w	662	650	8.76	1.38	16.54	Γ OH (33) + Γ CCCO(19) + Γ CCCC(28)
38			639	628	0.14	1.76	22.09	β CCO (56) + β CCN (11) + β CCCl (10)
39	611w		621	611	90.19	0.23	3.00	Γ OH (80)
40	590m	591w	599	589	6.98	1.27	17.37	β CCC(45) + β CCO (22) + υ C—Cl (11)
41	460s	482w	472	464	3.89	1.82	34.24	β CCN(34) + β COC(21) + υ C—Cl (14)
42			457	449	7.24	0.59	11.60	Γ CCCC(41) + Γ CCCH(18) + Γ CCNH(14) + Γ CCCO(10)
43		413m	421	414	148.04	2.55	55.947	Γ NH_{10} (85)
44			402	395	10.25	4.29	100.334	β CCO (76) + υ CC(11)
45		381s	380	374	95.30	3.72	93.762	Γ NH_{11} (60)
46		355m	366	360	7.97	9.15	243.08	υ C—COOH (50) + β CCC(27)
47		336w	338	333	51.88	1.95	57.742	Γ NH_{11} (35) + Γ CCCCl (18) + Γ CCCO (15)
48		302w	334	328	15.73	5.62	169.984	υ CCl (27) + β CCC (26) 10
49			277	272	1.90	1.88	74.315	β CCCl (36) + r NH_2 (33) + β C—COOH (14)
50			264	259	2.67	0.04	1.699	Γ CH_3 (53) + Γ CCCN (28)
51		225w	213	210	1.33	0.88	51.203	Γ CH_3 (44) + Γ CCCN (15) + Γ CCCCl (10)
52		197w	212	209	0.47	0.80	46.89	r CH_3 (73) + β $C_{18}CC$ (16)
53		183w	184	180	4.10	1.04	76.927	β CCCl (45) + r C—COOH (43)
54		113m	149	147	1.54	0.55	56.362	Γ CCCO (44) + Γ CCCCl (34)
55		71w	84	83	0.76	0.50	136.223	Γ CCCO (57) + ΓCCCC (15)
56			61	60	1.38	0.30	146.797	Γ CCO—CH_3 (76) + Γ O—CH_3 (12)
57			59	58	1.53	0.46	239.532	t COOH (90)

s-Strong, m-medium, w-weak, vs-very strong, vw-very weak, υ_{sym}: symmetric stretching, υ_{asym}: asymmetric stretching, β: in-plane bending, Γ: out-of-plane bending, ρ: scissoring, ω: wagging, t: twisting, r-rocking.

[a] I_{IR}: IR intensity.

[b] S_{Ra}: Raman scattering activity.

[c] I_{Ra}: Raman intensity, normalized to 100.

5.3.1. C—H vibrations

Aromatic compounds commonly exhibit multiple weak bands in the region 3100–3000 cm^{-1} due to aromatic C—H stretching vibrations [20–23]. The band appeared at 3071 cm^{-1} in FT-Raman spectrum is assigned to C—H ring stretching vibrations. The experimental bands identified at 3078, 3015 cm^{-1} for monomer and theoretical wavenumber at 3080, 3066 cm^{-1} by B3LYP method are assigned to C—H ring stretching vibrations. No bands are observed in FTIR spectrum. The TED contribution of 99% shows that they are pure stretching modes. All the C—H stretching vibrations are very weak in intensity and this is due to the decrease of dipole moment caused by the reduction of negative charge on the carbon atom. This reduction occurs because of the electron withdrawal on the carbon atom by the substituent due to the decrease of inductive

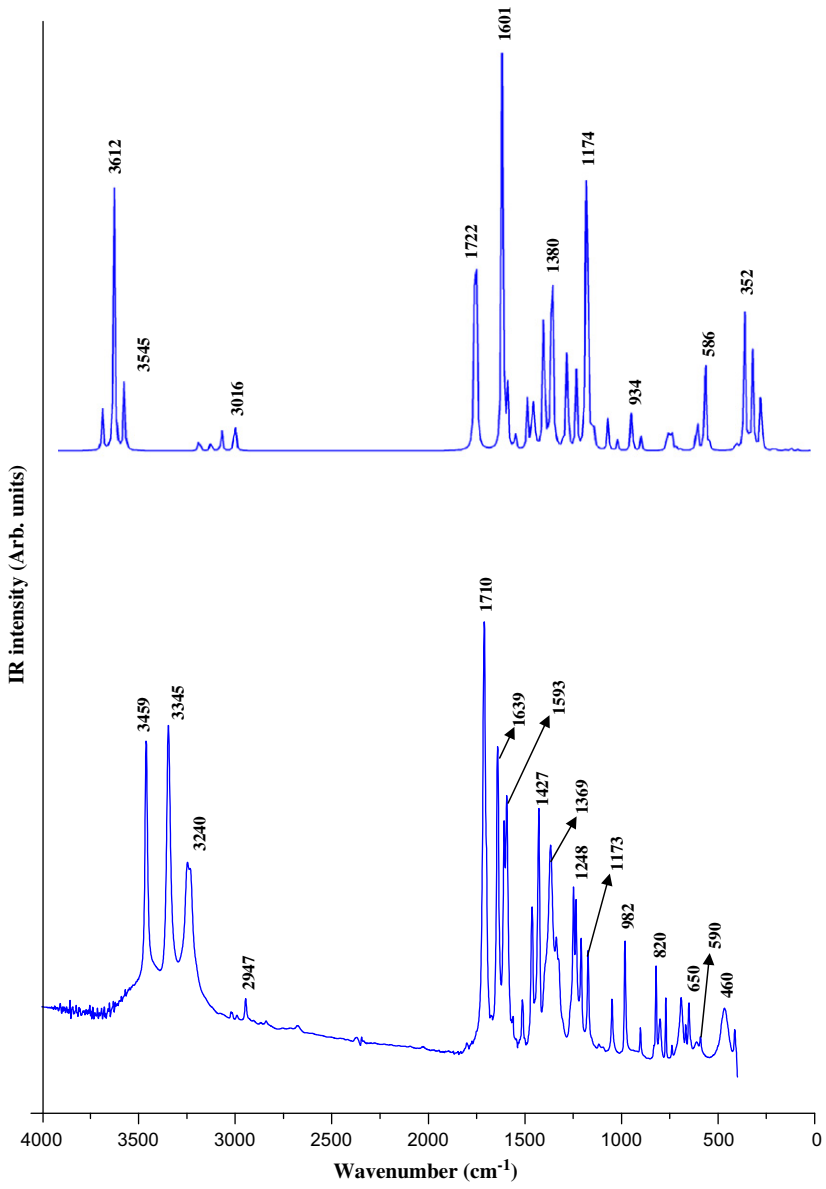

Fig. 3. Experimental (bottom) and theoretical (top) FTIR spectra of 4A5Cl2MBA.

effect, which in turn is caused by the increased chain length of the substituent [24].

The C—H in-plane and out-of-plane bending vibrations generally lie in the range 1000–1300 cm^{-1} and 950–800 cm^{-1} [25,26], respectively. In the present case, two C—H in-plane bending vibrations of the present compound identified at 1258, 1174 cm^{-1} for monomer are assigned to C—H in-plane bending vibrations. The same vibrations are measured in FTIR at 1248, 1173 cm^{-1} and in FT-Raman at 1265, 1195 cm^{-1}. The predicted vibrations are in line with the experimental data and literature value. The two C—H out-of-plane bending vibrations are observed at 902, 820 cm^{-1} in FTIR spectrum and at 903, 799 cm^{-1} in FT-Raman spectrum.

5.3.2. C—Cl vibrations

The presence of halogen on alkyl substituted aromatic ring can be detected indirectly from its electronic impact on the in-plane C—H bending vibrations [27]. The C—Cl stretching vibrations give generally strong bands in the region 730–580 cm^{-1} [28]. Mooney [29] assigned vibrations of C–X group (X = Cl, Br, I) in the frequency range of 1129–480 cm^{-1}. Accordingly, the bands observed in FTIR spectrum at 666, 460 cm^{-1} (mode No. 36 and 41) and in FT-Raman spectrum at 482 cm^{-1} are assigned to C—Cl stretching vibration. The predicted values (653, 464 cm^{-1} for monomer) show a small deviation ca. 1–10 cm^{-1} with experimental data and the maximum TED value is 18% as reported in Table 3. These vibrations are mixed with stretching and in-plane bending vibrations of C—C and C—O bond. The peaks at 272 and 180 cm^{-1} for monomer (183 cm^{-1}, in FT-Raman spectrum) are assigned to C—Cl in-plane-bending vibration whereas the out-of-plane bending C—Cl vibration is assigned to 113 cm^{-1} (FT-Raman), both are mixed vibrations as shown in Table 3. The remainder of the observed and calculated frequencies accounted in Table 3.

5.3.3. Amino group vibrations

The methylene and amino groups are generally referred to as electron donating substituents in aromatic ring system [30]. The CH_2 interacts with nearby π-systems via hyperconjugation, while the NH_2 share its lone pair of electrons with the π-electrons in a ring. Both mechanisms imply electronic delocalization and are taken into account by the molecular orbital approach. The molecule

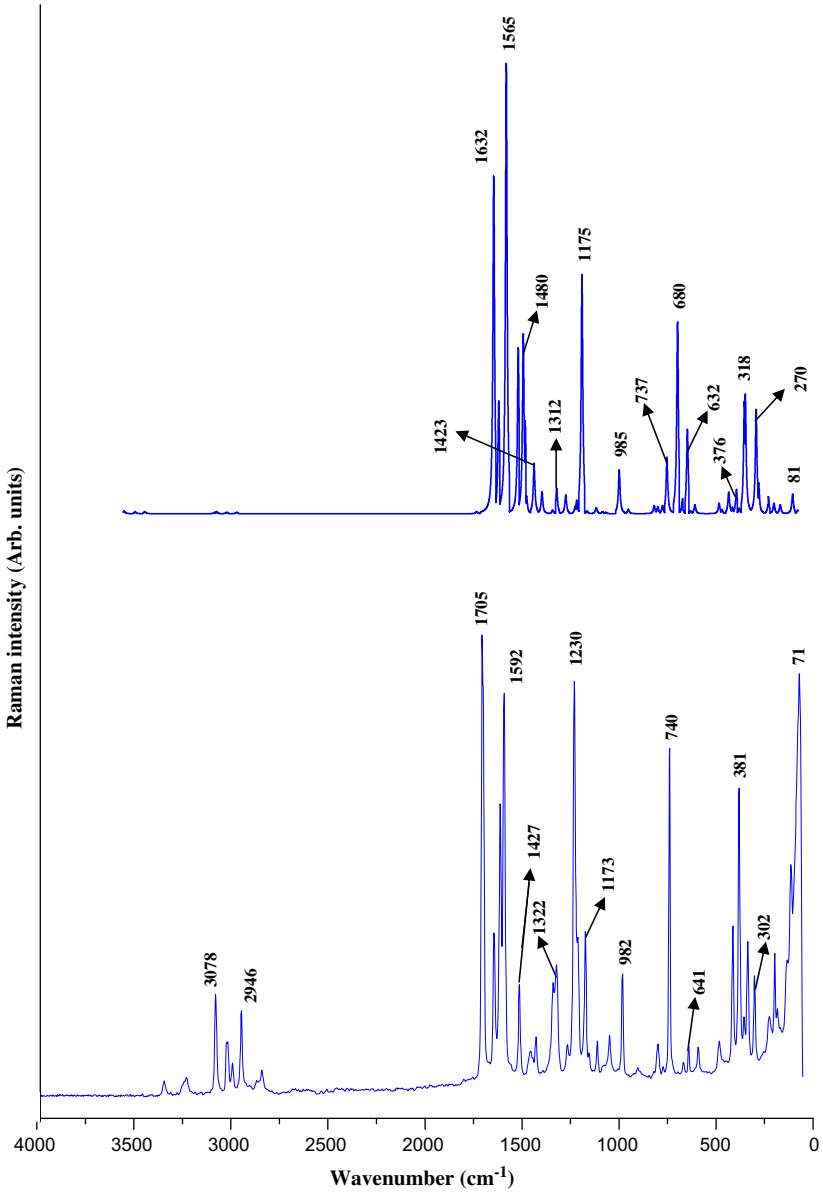

Fig. 4. Experimental (bottom) and theoretical (top) FT-Raman spectra of 4A5Cl2MBA.

under investigation possesses one NH_2 group and hence one can expect one asymmetric and one symmetric N—H stretching vibrations. It is stated that in amines, the N—H stretching vibrations occur in the region 3500–3300 cm^{-1}. The asymmetric-NH_2 stretching vibration appears from 3500 to 3420 cm^{-1} and the symmetric-NH_2 stretching is observed in the range 3420–3340 cm^{-1}. The antisymmetric (ν_{as}) stretching mode is calculated at the higher wavenumber 3545 cm^{-1} than the symmetric (ν_s) one at 3438 cm^{-1} by B3LYP/6-311++G(d,p) method having mode Nos. 1 and 3 as seen in Table 3. The infrared spectrum of title molecule shows a band observed at 3459 cm^{-1} corresponding to NH_2 asymmetric stretching mode. The symmetric stretching also observed as weak band in FTIR spectrum at 3240 cm^{-1}.

The scissoring mode of the NH_2 group appears in the region 1615–1650 cm^{-1} in benzene derivatives with NH_2 substituents. The calculated frequency for the scissoring mode of NH_2 is 1631 and 1605 cm^{-1} (mode Nos. 10 and 11) for monomer. This mode (mode Nos. 10 and 11) is also coupled with ring stretching mode as shown in Table 3. The computed vibrations well coincide with the experimental (1639, 1609 cm^{-1} in FTIR and 1643, 1612 cm^{-1} in FT-Raman) data. The theoretically predicted wavenumber by B3LYP method at 414, 374, 333 cm^{-1} is assigned to NH_2 out-of-plane bending vibrations.

5.3.4. COOH vibrations

The vibrational bands of the terminal —COOH groups of 4A5Cl2MBA contain the C—O, C═O and O—H vibrational modes. C═O stretching band appears strongly in the region 1870–1540 cm^{-1} in which the position of C═O stretching band depends on the physical state, electronic and mass effects of neighboring substituents, conjugations and intramolecular and intermolecular hydrogen bonding [31–33,22]. The C═O stretching mode is the strongest band in the infrared spectrum and appears with diminished intensity in the Raman spectrum. Hence the very strong FTIR band observed at 1710 cm^{-1} and FT-Raman band observed at 1705 cm^{-1} are assigned to the C═O stretching band of 4A5Cl2MBA molecule. The similar vibration is calculated for monomer at 1719 cm^{-1} by DFT-B3LYP method. However, the computed value

(1707 cm^{-1}) of C=O stretching vibration of monomer shows better agreement with the experimental data. In addition carboxylic acids also show C—O stretching band in FTIR at 1209 cm^{-1} and in FT-Raman at 1230 cm^{-1}.

As for the —OH hydroxyl group which connects the molecules, the observed IR frequency region is usually at the interval 3550–3200 cm^{-1} [33]. The O—H stretching vibration is observed in FTIR at 3345 cm^{-1} as shown in Fig. 3. Although these values are not observed in the recorded FT-Raman spectrum, the O—H stretching mode of monomer is found as 3488 cm^{-1} by B3LYP calculation level, as given in Table 3. Diverse dimeric units are common features among mono aminobenzoic acids as well as they are observed in the structure of benzoic acid [34]. The occurrence of dimeric conventions is due to hydrogen bonds which act as the bridging mode. The lower stretching frequency observed in 4A5Cl2MBA compared with the free O—H group stretching signifies that there is a possibility of intermolecular hydrogen bonding in 4A5Cl2MBA, between the hydroxyl group of one molecule and carbonyl group of another molecule. The carboxylic acid shows in-plane and out-of-plane bending vibrations of O—H group at 1369 and 650, 611 cm^{-1} (FTIR), respectively. The TED calculations show that the hydroxyl stretching vibrational mode is very pure. But the out-of-plane bending vibration of the hydroxyl group is overlapped with the other vibrations. The band due to the free hydroxyl group is sharp and its intensity increases.

5.3.5. Methoxy group vibrations

The wavenumbers of the vibrational modes of methoxy groups in 4A5Cl2MBA are known to be influenced by a variety of interesting interactions such as electronic effects, intermolecular hydrogen bonding in the crystalline network [35] and Fermi resonance. Electronic effects such as back-donation and induction, mainly caused by the presence of oxygen atom adjacent to CH_3 group, can shift the position of C—H stretching and bending modes [36–38]. Of this methoxy group of 4A5Cl2MBA, X-ray diffraction studies revealed that there is a weak intermolecular hydrogen formed between the $H_3C—O\cdots H—O$ of the hydroxyl group interaction play a key role in the formation of the crystalline network [39]. The C—H stretching vibrations in the methoxy group of bands observed in FTIR at 3019, 2947 and in FT-Raman at 3015, 2946 cm^{-1} are assigned to CH_3 asymmetric stretching vibrations. The theoretically scaled values by B3LYP/6-311++G(d,p) method at 3014, 2962 cm^{-1} (mode Nos. 6 and 7) are in good agreement with the experimental values. The theoretically predicted value at 2897 cm^{-1} is assigned to CH_3 symmetric stretching vibration. The Raman band at 1484 cm^{-1} is assigned to CH_3 scissoring vibration and is in excellent agreement with the theoretically calculated value by the B3LYP/6-31G(d) method at 1478 cm^{-1} (mode No. 14). The wagging mode of CH_3 group assigned at 1461, 1422 cm^{-1} for monomer shows good correlation with the measured wavenumbers 1460, 1427 cm^{-1} in FTIR and 1455, 1427 cm^{-1} in FT-Raman spectrum. Balafour [40] assigned the $O—CH_3$ torsional mode at 82 cm^{-1}, and Lakshmaiah and Rao [41] calculated this mode to be at 58 cm^{-1} for anisole. In our title molecule this mode calculated at 60 cm^{-1} is assigned to the $O—CH_3$ torsional mode.

5.3.6. Ring vibrations

The aromatic ring vibrational modes of title compound have been analyzed based on the vibrational spectra of previously published vibrations of the benzene molecule and they are helpful in the identification of the phenyl ring modes [30,42]. The ring stretching vibrations are very prominent, as the double bond is in conjugation with the ring, in the vibrational spectra of benzene and its derivatives [22]. The carbon–carbon stretching modes of the phenyl group are expected in the range from 1650 to 1200 cm^{-1}. The actual position of these modes is determined not so much by the nature of the substituents but by the form of substitution around the ring [43]. In general, the bands are of variable intensity and are observed at 1625–1590, 1590–1575, 1540–1470, 1465–1430 and 1380–1280 cm^{-1} from the wavenumber ranges given by Varsanyi [44] for the five bands in the region. In the present work, the wavenumbers observed in the FTIR spectrum at 1609, 1593, 1512, 1427, 1334 cm^{-1} and in FT-Raman spectrum at 1612, 1592, 1513, 1427, 1339, 1322 cm^{-1} have been assigned to C—C stretching vibrations. The theoretically computed values at 1605, 1566, 1504, 1422, 1326, 1305 cm^{-1} (monomer) show good agreement with experimental data. These modes are mixed modes with the contribution of C—H and C—N—H in-plane bending vibrations in this region. The C—C—C out-of-plane bending modes of monomer is attributed to the low wavenumbers computed at 734, 653, 589 cm^{-1} and these wavenumbers are consistent with the experimental wavenumbers.

5.4. ^{13}C and ^{1}H NMR spectral analysis

The relations between the calculated and experimental chemical shifts are linear and described by the following equation:

$$\delta_{cal.}(ppm) = 1.0444\delta_{\exp.} - 0.0548 \quad (R^2 = 0.9962)$$

$$^{1}H : \delta_{cal.}(ppm) = 0.7595\delta_{\exp.} + 1.3429 \quad (R^2 = 0.9067)$$

$$^{13}C : \delta_{cal.}(ppm) = 1.0208\delta_{\exp.} + 3.0939 \quad (R^2 = 0.9756)$$

The performances of the B3LYP method with respect to the prediction of the chemical shifts within the molecule were quite close. However, ^{13}C NMR calculations gave a slightly better coefficient and lower standard error (R^2 = 0.9756) than for ^{1}H NMR chemical shifts (R^2 = 0.9067). The measured ^{13}C, ^{1}H and DEPT NMR spectra are shown in Figs. 5–7. The computed and experimental ^{13}C NMR and ^{1}H NMR chemical shifts are tabulated in Table 4. Aromatic carbons give signals in overlapped areas of the spectrum with chemical shift values from 100 to 150 ppm [45,46]. In our present investigation, the experimental chemical shift values of aromatic carbons are in the range 98.28–160.12 ppm. As can be seen from Table 4, the calculated values show moderate agreement with measured values except the ^{1}H NMR chemical shifts of the active hydrogen atoms H10, H11 and H21 due to the influence of rapid proton exchange, hydrogen bond, solvent effect, etc. in the molecular system. The theoretically calculated chemical shifts of C5 and C6 atoms are found at 125.63 and 144.47 ppm respectively in DMSO solvent, which are largely downfield relative to aromatic benzene [47] due to the electronegative Cl atom which decrease the electron density of the adjacent carbon atoms of the ring.

The ^{13}C chemical shifts of carboxylic acids are in the range of 160–182 ppm but those of their salts between 167 and 183 ppm [48]. The experimental chemical shift value of C18 is 165.86 ppm and the calculated value is 171.71 ppm in gas phase and 167.64 ppm in DMSO solvent. The C18 and H21 atoms are deshielded due to the presence of electronegative oxygen in the carboxylic group.

5.5. Nonlinear optical effects

Nonlinear optical (NLO) effects arise from the interactions of electromagnetic fields in various media to produce new fields altered in phase, frequency, amplitude or other propagation characteristics from the incident fields [49]. NLO is at the forefront of current research because of its importance in providing the key functions of frequency shifting, optical modulation, optical switching, optical logic, and optical memory for the emerging technolo-

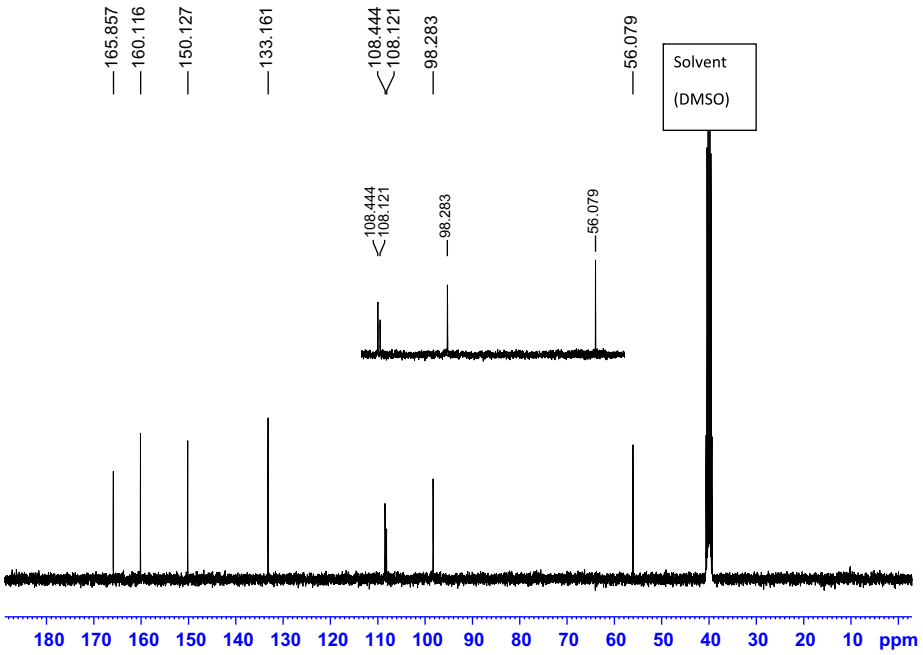

Fig. 5. Experimental ^{13}C NMR spectrum of 4A5Cl2MBA.

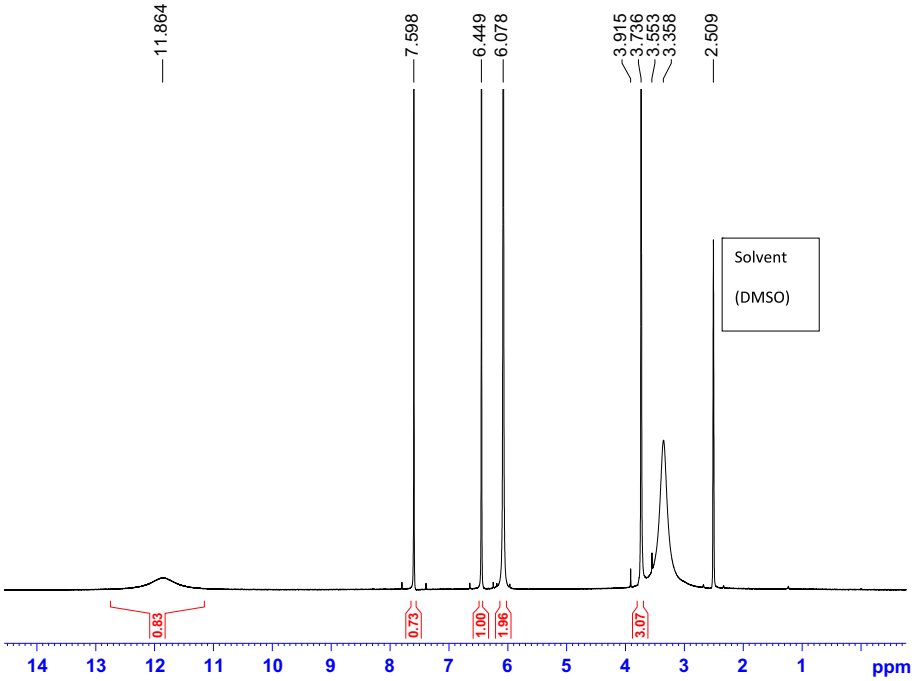

Fig. 6. Experimental ^{1}H NMR spectrum of 4A5Cl2MBA.

gies in areas such as telecommunications, signal processing, and optical interconnections [50–53].

The first hyperpolarizability (β_0) of this novel molecular system, and related properties (β, α_0 and $\Delta\alpha$) of 4A5Cl2MBA are calculated using B3LYP/6-311++G(d,p) method, based on the finite-field approach. In the presence of an applied electric field, the energy of a system is a function of the electric field. First order hyperpolarizability is a third rank tensor that can be described by $3 \times 3 \times 3$ matrices. The 27 components of the 3D matrix can be reduced to 10 components due to the Kleinman symmetry [54]. It can be given in the lower tetrahedral format. It is obvious that the lower part of the $3 \times 3 \times 3$ matrices is a tetrahedral. The components of β are defined as the coefficients in the Taylor series expansion of the energy in the external electric field. When the external electric field is weak and homogeneous, this expansion becomes:

$$E = E^0 - \mu_\alpha F_\alpha - 1/2\alpha_{\alpha\beta}F_\alpha F_\beta - 1/6\beta_{\alpha\beta\gamma}F_\alpha F_\beta F_\gamma + \cdots$$

where E^0 is the energy of the unperturbed molecules, F_α is the field at the origin, μ_α, $\alpha_{\alpha\beta}$ and $\beta_{\alpha\beta\gamma}$ are the components of dipole moment, polarizability and the first order hyperpolarizabilities, respectively. The total static dipole moment μ, the mean polarizability α_0, the

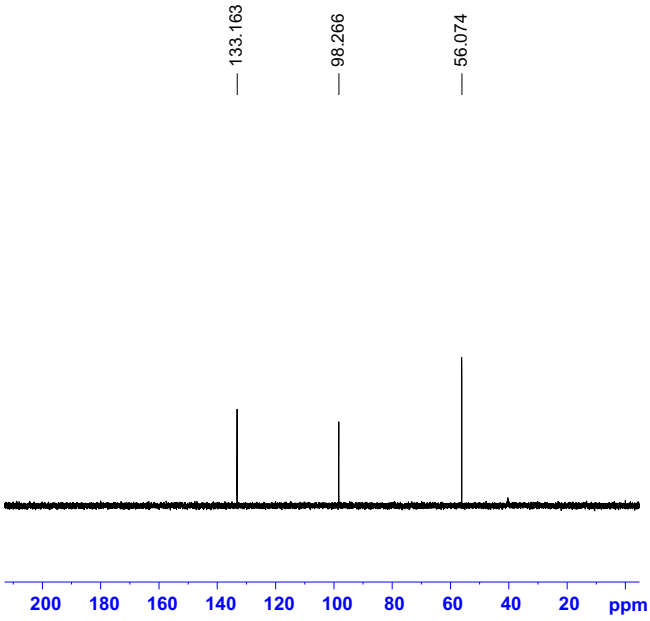

Fig. 7. Experimental DEPT NMR spectrum of 4A5Cl2MBA.

Table 4
Experimental and theoretical ^{1}H and ^{13}C isotropic chemical shifts (with respect to TMS) of 4A5Cl2MBA in DMSO and gas (all values in ppm).

Atom	Exp.	B3LYP		Atom	Exp.	B3LYP	
		DMSO	Gas			DMSO	Gas
H7	6.449	6.54	6.01	C1	108.121	113.67	115.86
H8	7.598	8.29	8.52	C2	160.116	165.67	168.23
H10	6.078	4.59	4.30	C3	98.283	97.24	101.54
H11	3.915	4.52	3.72	C4	150.127	154.48	158.14
H15	3.358	3.86	3.66	C5	108.444	125.63	124.81
H16	3.553	3.87	3.64	C6	133.161	144.47	142.52
H17	3.736	4.35	4.17	C14	56.079	56.54	58.30
H21	11.864	10.08	9.40	C18	165.857	167.64	171.71
Solvent	2.509			Solvent	39.500		

anisotropy of the polarizability $\Delta\alpha$ and the mean first order hyperpolarizability β_0, using the x, y, z components they are defined as:

$$\mu = (\mu_x^2 + \mu_y^2 + \mu_z^2)^{1/2}$$

$$\alpha_0 = (\alpha_{xx} + \alpha_{yy} + \alpha_{zz})/3$$

Table 5
The dipole moments μ (D), the polarizability α (a.u.), the average polarizability α_o (Å), the anisotropy of the polarizability $\Delta\alpha$ (Å), and the first hyperpolarizability β ($\times 10^{-30}$ cm^5 esu^{-1}) of 4A5Cl2MBA.

μ_x	0.74	β_{xxx}	−211.50
μ_y	3.41	β_{xxy}	−398.53
μ_z	−0.25	β_{xyy}	−258.99
μ_0	3.90	β_{yyy}	87.01
α_{xx}	172.81	β_{xxz}	47.84
α_{xy}	3.03	β_{xyz}	−33.44
α_{yy}	149.56	β_{yyz}	6.37
α_{xz}	0.31	β_{xzz}	88.64
α_{yz}	0.04	β_{yzz}	57.67
α_{zz}	71.59	β_{zzz}	64.29
α_0	19.46	β_x	−381.85
$\Delta\alpha$	46.40	β_y	−253.85
		β_z	118.50
		β	4.09

$$\alpha = 2^{-1/2}[(\alpha_{xx} - \alpha_{yy})^2 + (\alpha_{yy} - \alpha_{zz})^2 + (\alpha_{zz} - \alpha_{xx})^2 + 6\alpha^2 xx]^{1/2}$$

$$\beta_0 = (\beta_x^2 + \beta_y^2 + \beta_z^2)^{1/2}$$

and

$$\beta_x = \beta_{xxx} + \beta_{xyy} + \beta_{xzz}$$

$$\beta_y = \beta_{yyy} + \beta_{xxy} + \beta_{yzz}$$

$$\beta_z = \beta_{zzz} + \beta_{xxz} + \beta_{yyz}$$

Since the values of the polarizabilities (α) and hyperpolarizability (β) of the Gaussian 03 output are reported in atomic units (a.u.), the calculated values have been converted into electrostatic units (esu) (α: 1 a.u. = 0.1482×10^{-24} esu; β: 1 a.u. = 8.639×10^{-33} esu).

Urea is one of the prototypical molecules used in the study of the NLO properties of molecular systems. Therefore it was used frequently as a threshold value for comparative purposes. The total molecular dipole moment and the first order hyperpolarizability are 3.90 Debye and 4.0915×10^{-30} cm^5/esu, respectively and are depicted in Table 5. Total dipole moment of title molecule is approximately two and a half times greater than that of urea and the first order hyperpolarizability of title molecule is 11 times greater than that of urea (μ and β of urea are 1.3732 Debye and

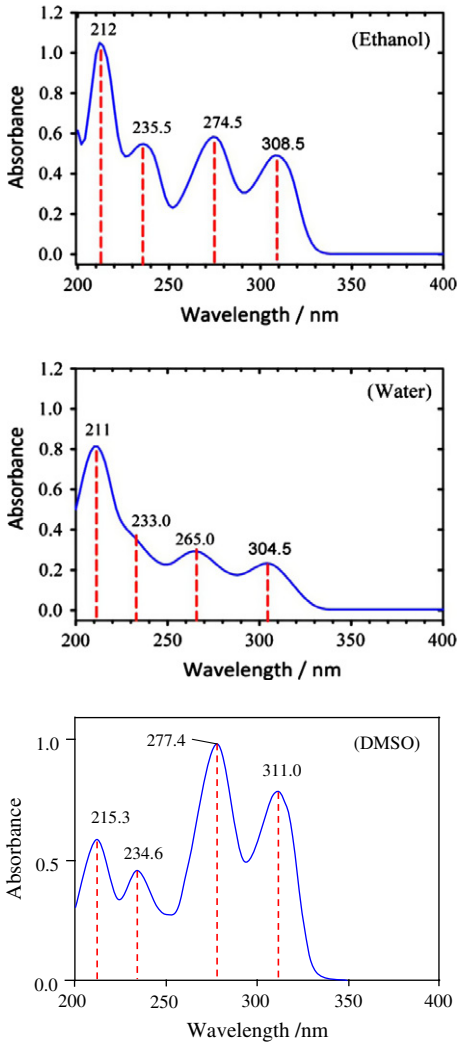

Fig. 8. Experimental UV spectra of 4A5Cl2MBA molecule in ethanol, water and DMSO solvent.

Table 6
Experimental absorption wavelength λ (nm), excitation energies E (eV) in solvent and computed absorption wavelength λ (nm), excitation energies E (eV) and oscillator strengths (f) of 4A5Cl2MBA in gas phase and in solvent (ethanol and water).

Experimental									TD-DFT/B3LYP/6-311++G(d,p)						
Ethanol		Water		DMSO		Gas			Ethanol			Water			
λ (nm)	E (eV)	λ (nm)	E (eV)	λ (nm)	E (eV)	λ (nm)	E (eV)	(f)	λ (nm)	E (eV)	(f)	λ (nm)	E (eV)	(f)	Assignment
308.5	4.0241	304.5	4.0770	311.0	4.0113	279.63	4.4339	0.1232	288.51	4.2974	0.2397	288.75	4.2939	0.2369	n–π*
274.5	4.5225	265.0	4.6847	277.4	4.2487	257.77	4.8099	0.0000	262.47	4.7237	0.1857	262.88	4.7164	0.1844	n–π*
						255.43	4.8540	0.0053	238.58	5.1967	0.2452	238.77	5.1927	0.2429	
						251.98	4.9204	0.1789	237.58	5.2186	0.0019	236.75	5.2369	0.0006	
235.5	5.2715	233.0	5.3280	234.6	5.0964	235.59	5.2626	0.0013	235.36	5.2678	0.0135	234.99	5.2762	0.0103	n–σ*
212.0	5.8558	211.0	5.8836		5.3286	228.52	5.4255	0.2172	229.46	5.4031	0.0013	229.34	5.4062	0.0015	n–π*

0.3728×10^{-30} cm^5/esu obtained by HF/6-311G(d,p) method). These results indicate that the title compound is a good candidate of NLO material.

To understand this phenomenon in the context of molecular orbital theory, we examined the molecular HOMOs and molecular LUMOs of the title compound. When we see the first hyperpolarizability value, there is an inverse relationship between the first hyperpolarizability and HOMO–LUMO gap, allowing the molecular orbitals to overlap to have a proper electronic communication conjugation, which is a marker of the intramolecular charge transfer

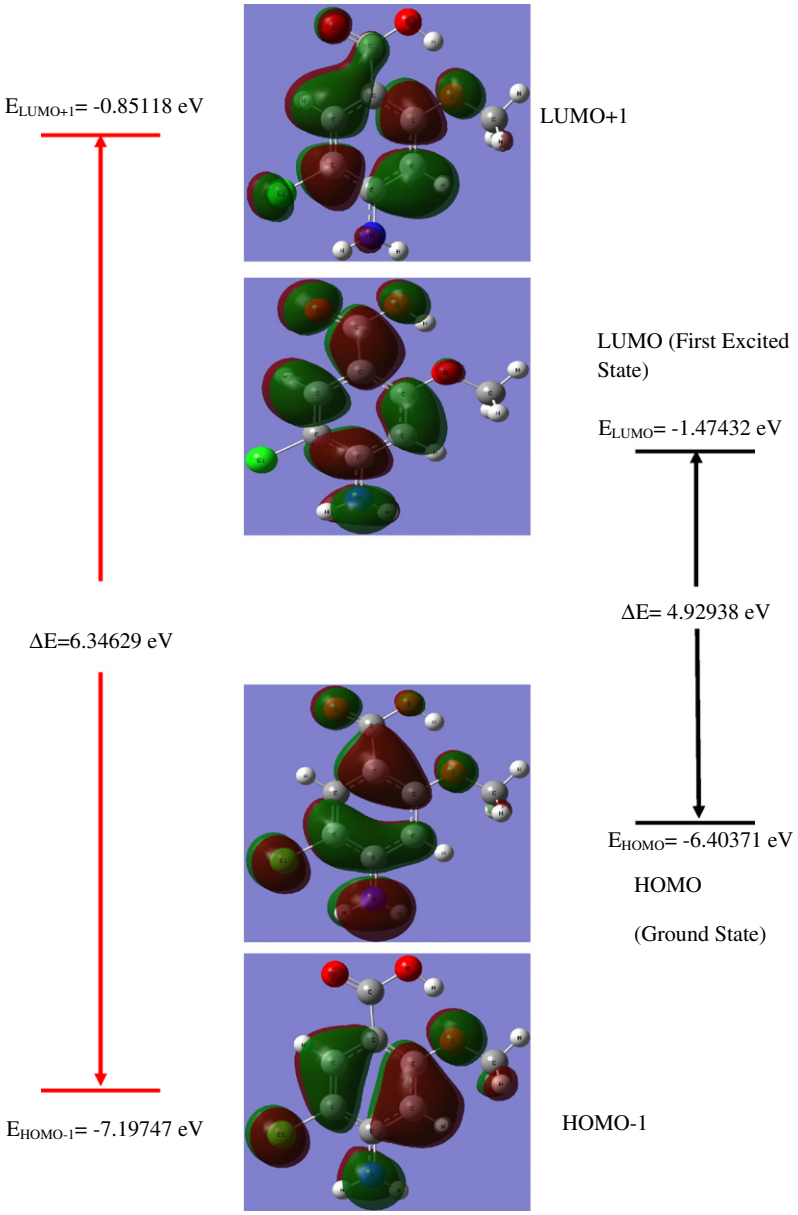

Fig. 9. The frontier and second frontier molecular orbitals of 4A5Cl2MBA.

from the electron donating group through the π-conjugation system to the electron accepting group [55,56].

5.6. UV–Vis spectral analysis

The electronic absorption spectra of the title compound in ethanol, water and DMSO solvent were recorded within the 200–400 nm range and representative spectra are shown in Fig. 8. As can be seen from the Fig. 8, electronic absorption spectra showed four bands at 308.5, 274.5, 235.5 and 212.0 nm for ethanol, at 304.5, 265.0, 233.0 and 211.0 nm for water and at 311.0, 277.4 and 234.6 nm for DMSO medium. The band at 215.3 nm in DMSO medium may be due to solvent peak. Electronic absorption spectra were calculated using the TD-DFT method based on the B3LYP/6-311++G(d,p) level optimized structure in gas phase. The calculated results are listed in Table 6 along with the experimental absorption spectral data. For TD-DFT calculations, the theoretical absorption bands are predicted at 279.63, 257.77, 255.43, 251.98, 235.59 and 228.52 nm in gas phase. In addition to the calculations in gas phase, TD-DFT calculations of the title compound in ethanol and water as solvent were performed using the PCM model. The PCM calculations reveal that the calculated absorption bands have slight red-shifts with the values of 288.51, 262.47, 235.36 nm in ethanol and 288.75, 262.88, 234.99 nm in water comparing with the gas phase calculations of TD-DFT method. And also, the calculated bands have slight blue-shift with the values of 229.46 nm and 229.34 nm in ethanol and water respectively. The band at 308.5 nm (ethanol), 304.5 nm (water) and 311.0 nm (DMSO) is assigned as n–π* transition. Similarly, the band at 235.5 nm (ethanol), 233.0 nm (water) and 234.6 nm (DMSO) is assigned to n–π* transition. Thus, the TD-DFT method in the gas phase and in solvent media is convenient for predicting electronic absorption spectra.

5.7. HOMO–LUMO analysis

Molecular orbital and their properties like energy are very useful to the physicists and chemists and their frontier electron density used for predicting the most reactive position in π-electron system and also explained several types of reaction in conjugated systems [57]. The total energy, energy gap and dipole moment affect the stability of a molecule. Surfaces for the frontier orbital were drawn to understand the bonding scheme of present compound and it is shown in Fig. 9. The conjugated molecules are characterized by a highest occupied molecular orbital-lowest unoccupied molecular orbital (HOMO–LUMO) separation, which is the result of a significant degree of intermolecular charge transfer (ICT) from the end-capping electron-donor to the efficient electron acceptor group through π-conjugated path. The HOMO is the orbital that primarily acts as an electron donor and the LUMO is the orbital that largely acts as the electron acceptor, and the gap between HOMO and LUMO characterizes the molecular chemical stability. The energy gap between the HOMO and the LUMO molecular orbitals is a critical parameter in determining molecular electrical transport properties because it is a measure of electron conductivity. The HOMO is delocalized over the entire molecule except methyl group. The HOMO → LUMO transition implies an electron density transfer to carboxyl group through benzene ring from amino group and chlorine atom. The computed energy values of HOMO and LUMO are −6.40371 eV and −1.47432 eV, respectively. The energy gap value is 4.92938 eV in ethanol for 4A5Cl3MBA molecule. The energy values of the frontier orbitals are presented in Table 7. The energy gap between HOMO and LUMO determines the kinetic stability, chemical reactivity and, optical polarizability and chemical hardness–softness of a molecule [58].

Table 7
Calculated energies values of 4A5Cl2MBA.

RTD-DFT/B3LYP/6-311++G(d,p)	Gas	Ethanol	Water
E_{total} (Hartree)	−1050.3386	−1050.3614	−1050.3624
E_{HOMO} (eV)	−6.4037	−6.3297	−6.3281
E_{LUMO} (eV)	−1.4743	−1.5641	−1.5717
$\Delta E_{HOMO-LUMO\ gap}$ (eV)	4.9294	4.7656	4.7563
E_{HOMO-1} (eV)	−7.1975	−7.0315	−7.0250
E_{LUMO+1} (eV)	−0.8512	−0.6868	−0.6846
$\Delta E_{HOMO-1-LUMO+1\ gap}$ (eV)	6.3463	6.3447	6.3403
Dipole moment (Debye)	4.5056	7.4502	7.5620

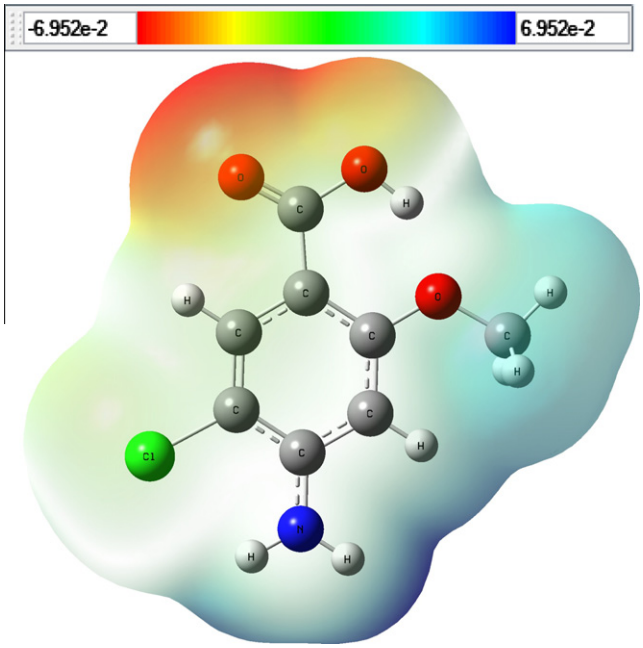

Fig. 10. Molecular electrostatic potential map (MEP) of 4A5Cl2MBA molecule.

5.8. Molecular electrostatic potential

Molecular electrostatic potential (MEP) at a point in the space around a molecule gives an indication of the net electrostatic effect produced at that point by the total charge distribution (electron + nuclei) of the molecule and correlates with dipole moments, electronegativity, partial charges and chemical reactivity of the molecules. It provides a visual method to understand the relative polarity of the molecule. Fig. 10 provides a visual representation of the chemically active sites and comparative reactivity of atoms. The different values of the electrostatic potential at the surface are represented by different colors. Potential increases in the order red < orange < yellow < green < blue. The color code of these maps is in the range from −43.6244 kcal/mol (deepest red) to +43.6244 kcal/mol (deepest blue) in the compound, where blue indicates the strongest attraction and red indicates the strongest repulsion. As can be seen from the MEP map of the title molecule, while regions having the negative potential are over the electronegative atom (Oxygen and chloro atoms), the regions having the positive potential are over the hydrogen atoms. The negative potential value is −43.6244 kcal/mol for oxygen atom (C=O for oxygen atom, O19). A maximum positive region localized on the H atom bond has value of +43.6244 kcal/mol (NH_2 for H atom, H11).

6. Conclusions

The FTIR, FT-Raman spectra, ^1H, ^{13}C NMR and UV–Visible spectra of 4-amino-5-chloro-2-methoxybenzoic acid have been recorded

and analyzed. The equilibrium geometries, harmonic wavenumbers for monomer and dimer calculations (conformer 1) have been carried out for the first time at DFT level. Optimized geometrical parameters of the title compound are in agreement with the crystal structure data obtained from XRD studies. Ab initio programs were used to find the most stable conformer of 4A5Cl2MBA. In the present study, experimental and calculated vibrational wavenumber analysis confirms the existence of dimer by involvement of heteronuclear association through carbonyl (C═O) oxygen and hydroxyl (O—H) hydrogen of acid group. Theoretical electronic absorption spectra have some blue shifts compared with the experimental data and molecular orbital coefficients analysis suggests that electronic transitions are assigned to π–π^* type. The theoretically constructed FTIR and FT-Raman spectra exactly coincide with experimentally observed counterparts.

References

[1] S. Kanchan, D.N.S. Jayachandra, Can. J. Bot. 59 (1981) 199.
[2] J.F. Lynas, B. Walker, Bioorg. Med. Chem. Lett. 7 (1997) 1133.
[3] S. Minatchy, N. Mathew, Ind. J. Chem. 37B (1998) 1066.
[4] R. Fausto, A. Matos-Beja, J.A. Paixao, J. Mol. Struct. 435 (1997) 207.
[5] M. Samsonowicz, T. Hrynaszkiewicz, R. Swisłocka, E. Regulska, W. Lewandowski, J. Mol. Struct. 744–747 (2005) 345.
[6] N. Sundaraganesan, B. Dominic Joshua, K. Settu, Spectrochim. Acta 66A (2007) 381.
[7] N. Sundaraganesan, B. Anand, C. Meganathan, B.D. Joshua, Spectrochim. Acta 69A (2008) 871.
[8] M. Kalinowska, G. Swiderski, W. Lewandowski, Polyhedron 28 (2009) 2206.
[9] Gaussian Inc., Gaussian 03 Program, Gaussian Inc.: Wallingford, 2004.
[10] A.D. Becke, J. Chem. Phys. 98 (1993) 5648.
[11] A.D. Becke, J. Chem. Phys. 107 (1997) 8554.
[12] C. Lee, W. Yang, C.R. Parr, Phys. Rev. B 37 (1988) 785.
[13] W.J. Hehre, L. Random, P.V.R. Schleyer, J.A. Pople, Ab Initio Molecular Orbital Theory, Wiley, New York, 1989.
[14] R. Dennington II, T. Keith, J. Millam, Gauss View, Version 4.1.2, Semichem, Inc., Shawnee Mission, KS, 2007.
[15] M.H. Jamróz, Vibrational Energy Distribution Analysis VEDA 4, Warsaw, 2004.
[16] K. Wolonski, J.F. Hinton, P. Pulay, J. Am. Chem. Soc. 112 (1990) 8251.
[17] G. Keresztury, S. Holly, J. Varga, G. Besenyei, A.Y. Wang, J.R. Durig, Spectrochim. Acta 9A (1993) 2007.
[18] G. Keresztury, in: J.M. Chalmers, P.R. Griffith (Eds.), Raman Spectroscopy: Theory, Hand book of Vibrational Spectroscopy, vol. 1, John Wiley & Sons Ltd., New York, 2002.
[19] N. Sundaraganesan, S. Ilakiamani, H. Saleem, P.M. Wojciechowski, D. Michalska, Spectrohim. Acta 61A (2005) 2995.
[20] V. Krishnakumar, V. Balachandran, T. Chithambarathanu, Spectrochim. Acta 62A (2005) 918.
[21] N. Puviarasan, V. Arjunan, S. Mohan, Turk. J. Chem. 26 (2002) 323.
[22] G. Varsanyi, Vibrational Spectra of Benzene Derivatives, Academic Press, New York, 1969.
[23] V. Krishnakumar, R. John Xavier, Indian J. Pure Appl. Phys. 41 (2003) 597.
[24] H. Spedding, D.H. Whiffen, Proc. Roy. Soc. Lond. A 238 (1956) 245.
[25] V. Krishnakumar, V.N. Prabavathi, Spectrochim. Acta, Part A 71 (2008) 449.
[26] A. Altun, K. Golcuk, M. Kumru, J. Mol. Struct. 637 (2003) 155.
[27] J. Coates, Interpretation of Infrared Spectra—A Practical Approach, in: Encyclopedia of Analytical Chemistry, John Wiley & Sons, Ltd., Chichester, 2000. pp. 10815.
[28] P.B. Nagabalasubramanian, S. Periandy, S. Mohan, Spectrochim. Acta 73A (2009) 277.
[29] E.F. Mooney, Spectrochim. Acta 20 (1964) 1021.
[30] N.B. Colthup, L.H. Daly, S.E. Wiberley, Introduction to Infrared and Raman Spectroscopy, Academic Press, New York, 1990.
[31] B.H. Stuart, Infrared Spectroscopy: Fundamentals and Applications, John Wiley & Sons, England, 2004.
[32] S. Chandra, H. Saleem, N. Sundaraganesan, S. Sebastian, Spectrochim. Acta A74 (2009) 704.
[33] R.M. Silverstein, F.X. Webster, Spectroscopic Identification of Organic Compound, sixth ed., John Willey & Sons, New York, 1998.
[34] A. Pawlukoj, J. Leciejewicz, Chem. Phys. 229 (2004) 39.
[35] V. Shettigar, P.S. Patil, S. Naveen, S.M. Dharmaprakash, M.A. Sridhar, J. Shashidhara Prasad, J. Cryst. Growth 305 (2007) 218.
[36] M. Gussoni, C. Castiglioni, J. Mol. Struct. 651 (2003) 151.
[37] J. Palomar, J.L.G. De Paz, J. Catalan, Chem. Phys. 246 (1999) 167.
[38] M. Rumi, G. Zerbi, J. Mol. Struct. 509 (1999) 11.
[39] Y. Qu, X.M. Sun, Acta Crystallogr. E 61 (2005) 3828.
[40] J.W. Balafour, Spectrochim. Acta 39A (1983) 795.
[41] B. Lakshmaiah, G.R. Rao, Appl. Phys. 29 (1991) 370.
[42] G. Socrates, Infrared Characteristic Group frequencies, Wiley-Interscience Publication, New York, 1980.
[43] L.J. Bellamy, The Infrared Spectra of Complex Molecules, third ed., Wiley, New York, 1975.
[44] G. Varsanyi, Assignments of Vibrational Spectra of Seven Hundred Benzene Derivatives, vols. 1–2, Adam Hilger, 1974.
[45] H.O. Kalinowski, S. Berger, S. Braun, Carbon-13 NMR Spectroscopy, John Wiley & Sons, Chichester, 1988.
[46] K. Pihlaja, E. Kleinpeter (Eds.), Carbon-13 Chemical Shifts in Structural and Sterochemical Analysis, VCH Publishers, Deerfield Beach, 1994.
[47] Y.X. Zhao, X.Y. Sun, Spectroscopic Identification of Organic Structures, Science Press, 2010. pp. 278.
[48] F. Pretsch, P. Bühlman, C. Affolter, Structure determination of organic compounds, in: Tables of Spectral Data, Springer-Verlag, Berlin, 2000.
[49] Y.X. Sun, Q.L. Hao, W.X. Wei, Z.X. Yu, L.D. Lu, X. Wang, Y.S. Wang, J. Mol. Struct.: Theochem 904 (2009) 74.
[50] C. Andraud, T. Brotin, C. Garcia, F. Pelle, P. Goldner, B. Bigot, A. Collet, J. Am. Chem. Soc. 116 (1994) 2094.
[51] V.M. Geskin, C. Lambert, J.L. Bredas, J. Am. Chem. Soc. 125 (2003) 15651.
[52] M. Nakano, H. Fujita, M. Takahata, K. Yamaguchi, J. Am. Chem. Soc. 124 (2002) 9648.
[53] D. Sajan, I.H. Joe, V.S. Jayakumar, J. Zaleski, J. Mol. Struct. 785 (2006) 43.
[54] D.A. Kleinman, Phys. Rev. 126 (1962) 1977.
[55] M.C. Ruiz Delgado, V. Hernandez, J. Casado, J.T. Lopez Navarre, J.M. Raimundo, P. Blanchard, J. Roncali, J. Mol. Struct. 151 (2003) 651.
[56] J.P. Abraham, D. Sajan, V. Shettigar, S.M. Dharmaprakash, I. Nemec, I.H. Joe, V.S. Jayakumar, J. Mol. Struct. 917 (2009) 27.
[57] K. Fukui, T. Yonezawa, H. Shingu, J. Chem. Phys. 20 (1952) 722.
[58] B. Kosar, C. Albayrak, Spectrochim. Acta 78A (2011) 160.